Journal of Biomechanics 43 (2010) 1623–1626

Contents lists available at ScienceDirect

Journal of Biomechanics

journal homepage: www.elsevier.com/locate/jbiomech
www.JBiomech.com

Short communication

Automatic determination of anatomical coordinate systems for three-dimensional bone models of the isolated human knee

Daniel L. Miranda [a], Michael J. Rainbow [a], Evan L. Leventhal [a], Joseph J. Crisco [a,b], Braden C. Fleming [a,b,*]

[a] Bioengineering Laboratory, Department of Orthopaedics, The Warren Alpert Medical School of Brown University/Rhode Island Hospital, CORO West, Suite 404, 1 Hoppin Street, Providence, RI 02903, USA
[b] Division of Engineering, Brown University, Providence, RI, USA

ARTICLE INFO

Article history:
Accepted 14 January 2010

Keywords:
Knee
Kinematics
Anatomical coordinate system
Three-dimensional model
Surface fitting

ABSTRACT

The combination of three-dimensional (3-D) models with dual fluoroscopy is increasingly popular for evaluating joint function *in vivo*. Applying these modalities to study knee motion with high accuracy requires reliable anatomical coordinate systems (ACSs) for the femur and tibia. Therefore, a robust method for creating ACSs from 3-D models of the femur and tibia is required. We present and evaluate an automated method for constructing ACSs for the distal femur and proximal tibia based solely on 3-D bone models. The algorithm requires no observer interactions and uses model cross-sectional area, center of mass, principal axes of inertia, and cylindrical surface fitting to construct the ACSs. The algorithm was applied to the femur and tibia of 10 (unpaired) human cadaveric knees. Due to the automated nature of the algorithm, the within specimen variability is zero for a given bone model. The algorithm's repeatability was evaluated by calculating variability in ACS location and orientation across specimens. Differences in ACS location and orientation between specimens were low (<1.5 mm and $<2.5^{\circ}$). Variability arose primarily from natural anatomical and morphological differences between specimens. The presented algorithm provides an alternative method for automatically determining subject-specific ACSs from the distal femur and proximal tibia.

1. Introduction

Accurate bone-based coordinate systems are critical for studying the effect of kinematics on ligament and articular cartilage deformation (Andriacchi et al., 2004, 2009; Andriacchi and Mündermann, 2006; Jordan et al., 2007). X-ray-based three-dimensional (3-D) skeletal motion-capture technologies require reliable methods for establishing femoral and tibial anatomical coordinate systems (ACSs) to measure knee kinematics.

Standard methods for defining femoral and tibial ACSs use the knee, hip, and ankle joints. Typically, the knee's flexion–extension (FE) axis is defined as the vector through a cylinder fitted to the femoral condyles. Additional axes are built using the center of the femoral head. The tibial ACS is traditionally defined using medial and lateral points on the tibial plateau combined with the ankle's center (Eckhoff et al., 2005; Fernandez et al., 2008).

An alternative method is necessary for *ex vivo* biomechanical studies using isolated knee preparations that do not include the proximal femur and distal tibia. Ideally, the method could be used both *in vivo* and *ex vivo*. Herein, we present and evaluate an automated method for constructing subject-specific ACSs for the distal femur and proximal tibia based on bony geometry derived from 3-D images (Fig. 1).

2. Methods

2.1. Bone models

CT images of the distal femur and proximal tibia of 10 fresh frozen cadaver knees (7 right, 3 left; 7 male, 3 female, aged 58.3 ± 11.1 years) were acquired (80 kVp, 400 mA, $0.22 \times 0.22 \times 0.625 \text{mm}^3$; LightSpeed, GE). CT-based 3-D bone models were then generated using Materialise Mimics 12.01.

2.2. Femoral ACS

The primary axis of the femoral ACS (medial–lateral, ML) was established from its articulating surfaces. The femoral condyles were isolated using a plane oriented over two iterations. This was done to align the plane's ML axis with the distal femur's anatomy to evenly capture the articulating surfaces (Fig. 2A.1). A cylinder was fit to the condyles using a Matlab-based Gauss–Newton algorithm (Fig. 2B). The cylinder's center vector formed the ML axis of the femoral ACS because it approximates the knee's FE axis (Eckhoff et al., 2005; Morrison, 1970; Pennock and Clark, 1990).

The normal vector defining the plane's first iteration was determined by crossing a vector connecting a point on the distal femur (pt_1) and a point on the posterior femur (pt_2) with a vector pointing in the ML direction. This vector was

* Corresponding author at: Bioengineering Laboratory, Department of Orthopaedics, The Warren Alpert Medical School of Brown University/Rhode Island Hospital, CORO West, Suite 404, 1 Hoppin Street, Providence, RI 02903, USA. Tel.: +1 401 444 4416; fax: +1 401 444 4418.
E-mail address: Braden_Fleming@brown.edu (B.C. Fleming).

0021-9290/$ - see front matter © 2010 Elsevier Ltd. All rights reserved.
doi:10.1016/j.jbiomech.2010.01.036

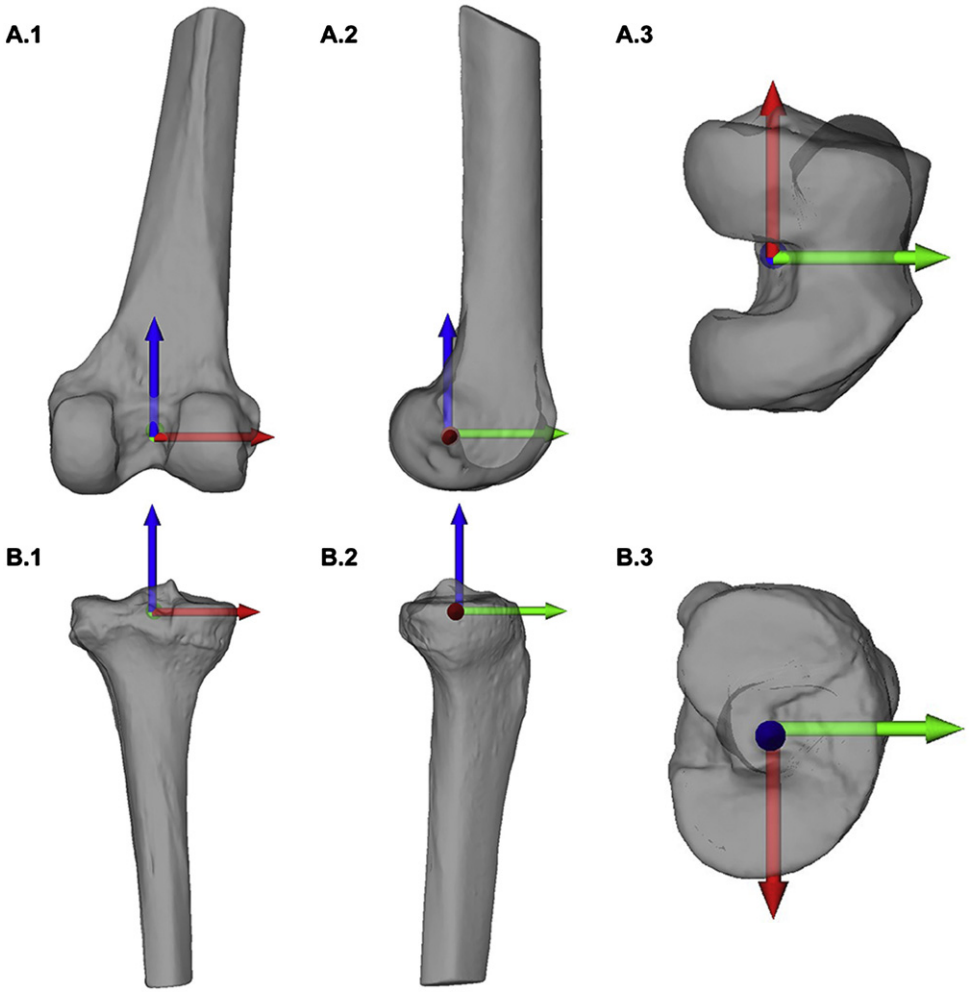

Fig. 1. The algorithm begins with 3-D models of the distal femur and proximal tibia generated from a CT scan of the knee. Initial inertial axes are used to isolate the femoral diaphysis, femoral condyles, and tibial plateau. (A) The ML axis of the femoral ACS is determined by fitting a cylinder to the condyles. The AP axis of the femoral ACS is calculated by crossing the ML axis with the inertial axis aligned along the femoral diaphyseal's length. The long axis of the femoral ACS is calculated by re-crossing the AP axis with the ML axis. (B) The three axes of the tibial ACS are defined using the isolated plateau's inertial axes.

defined using the femur's inertial axes (Gonzalez-Ochoa et al., 1998). The points isolated from the plane's first iteration were fit with a cylinder. The cylinder's center vector was used to define a new ML vector. The normal vector defining the plane's final iteration was determined by crossing the new ML vector with the vector connecting pt_1 and pt_2.

pt_1 was determined by extending a vector distally through the femoral diaphysis until it intersected with the femur (Fig. 2A.1, A.2). The smallest inertial axis of only the femoral diaphysis defined this vector. The diaphysis was isolated by calculating the femur's inertial axes. Axial cross-sections oriented using these axes were determined along the femur's length (Fig. 3). Three locations were determined along the smallest inertial axis of the femur: (1) the maximum cross-sectional area; (2) half the maximum cross-sectional area; and (3) 30% farther from the distal end of the femur than the second location. Finally, a plane oriented using the femur's inertial axes and positioned at the third location was used to isolate the diaphysis.

pt_2 was established using the previously described axial cross-sections. A plane at the second location, oriented using the femur's inertial axes, was used to determine the center of a box bounding the femur (Fig. 2A.3). Finally, pt_2 was determined by extending the femur's inertial axis pointing in the anterior–posterior (AP) direction through the posterior femur.

The femoral ACSs secondary axis (AP) was calculated by crossing the vector through the diaphysis with the ML axis. The femoral ACSs third axis was calculated by re-crossing the AP and ML axes. The origin of the femoral ACS was positioned at the centroid of the cylinder fit to the condyles.

2.3. Tibial ACS

The articulating surface of the tibial plateau was used to define the ML, AP, and third axes of the tibial ACS. The plateau was isolated by calculating the tibia's inertial axes. A plane oriented using the tibia's inertial axes and positioned at the largest cross-sectional area was used to isolate the plateau. The inertial axes of only the plateau were designated as the ML, AP, and third axes of the tibial ACS. The origin of the tibial ACS was positioned at the plateau's center of mass.

2.4. Data analysis

The algorithm's repeatability was evaluated by computing the differences in location and orientation of each ACS after aligning each bone to a template bone using a surface registration protocol. Prior to registration, the bone models were scaled to similar volumes according to a scale factor determined by balancing the width of each specimen's condyles or tibial plateau. Femoral and tibial surface registrations were then performed using Geomagic Studio's (v10) best-fit alignment algorithm.

3. Results

The described algorithm was successful in automatically constructing ACSs for the femur and tibia from the CT-based bone models. The algorithm's repeatability was evaluated by computing the differences in location and orientation of each ACS compared to the mean ACS, which was determined for both by averaging each specimen's axes and origins. Location differences were evaluated as 2-D component (x, y, z) distances and absolute 3-D distances. Orientation differences were evaluated as angular ACS x-, y-, and z-axis distances. Mean femoral and tibial ACS x-, y-, and z-location and orientation differences were consistent, with a

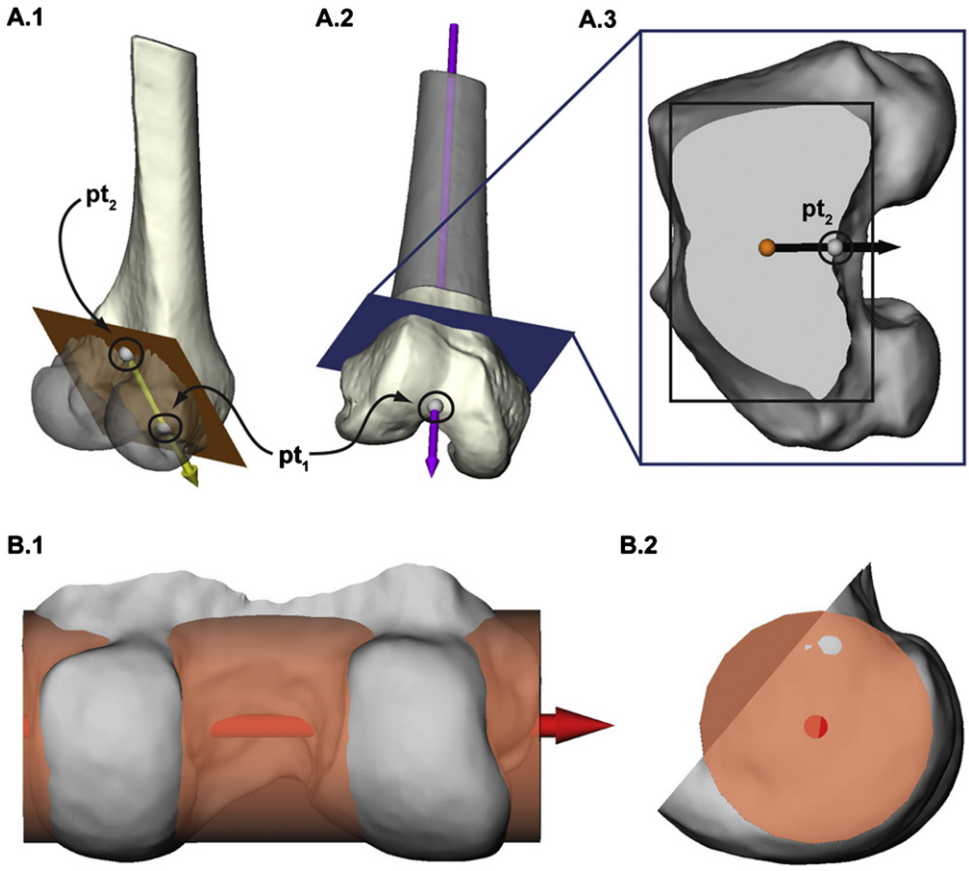

Fig. 2. (A.1) Posterior view of the plane used to isolate to the condyles. The yellow arrow represents the vector connecting pt_2 to pt_1. (A.2) Anterior view of the vector through the diaphysis (purple arrow). The intersection of this vector with the distal femur defined pt_1. The axial plane placed within the metaphysis was used to determine pt_2. (A.3) Top view of the axial cross-section of the femoral metaphysis. The orange sphere is the center of the box bounding the femur. The black arrow represents the femurs inertial axis pointing in the AP direction placed at the center of the femoral bounding box. The intersection of this vector with the posterior femur defined pt_2. (B.1) Distal view of the condyles. (B.2) Lateral view of the condyles. The cylinder is fit to the condyles using a least-squares algorithm. The condyles were isolated using the second iteration of the plane shown in (A.1). The red arrow is the vector through the center of the cylinder, denoted as the ML axis of the femoral ACS.

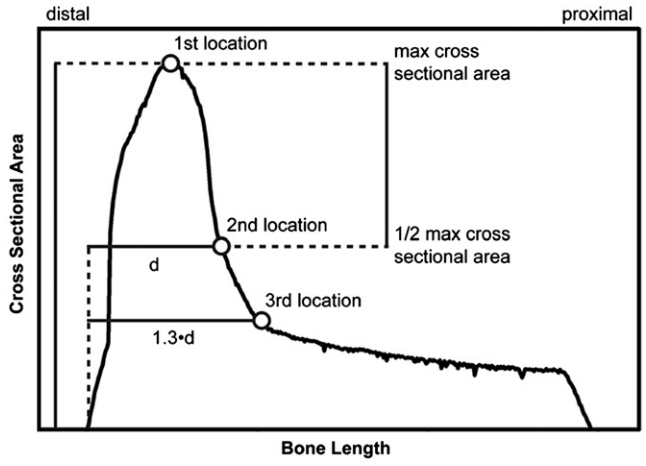

Fig. 3. Representative graph showing cross-sectional area versus bone length. Cross-sectional area was used to define three locations along the length of the bone that were used to isolate the femoral condyles, diaphysis, and tibial plateau. The first location was positioned at the maximum cross-sectional area. The second location was positioned a distance (d) from the distal end of the femur. The distance (d) was determined by half the maximum cross-sectional area. The third location was set 30% farther from the distal end of the femur than the second location. The placement of these locations was based on preliminary evaluations of consistency across specimens. The locations were appropriate for all tested femurs and their placement did not vary. Small variations did not significantly alter the ACS definitions.

bias of less than 1.5 mm and 2.5° (Fig. 4). Additionally, the femoral ACS's average absolute 3-D location difference was slightly larger (1.7 mm) with a more dispersed range (CI: 1.3–2.2 mm) than the tibial ACSs (1.1 mm, CI: 0.7–1.5 mm).

4. Discussion

We have presented an automated method for constructing subject-specific ACSs for the distal femur and proximal tibia based solely on their 3-D bony geometry. The algorithm was automated to eliminate time-consuming user interactions that may introduce theoretical bias from point or region selection. The ACSs were designed to define a knee joint coordinate system (JCS) based on a geometrical model of the femur's cylindrical surface rolling on top of the tibia's planar surface (Morrison, 1970; Pennock and Clark, 1990). Describing this motion using two right-handed orthogonal coordinate systems allows angulations between the femur and tibia to be captured in all three anatomical planes.

Traditional methods for defining femoral and tibial ACSs employ data from the hip and ankle joints that may not be available for *ex vivo* biomechanics studies of isolated knee preparations (Eckhoff et al., 2005; Fernandez et al., 2008). Aspects of previous axis definitions were translated to the presented algorithm. Specifically, the axis of the cylinder fit to the femoral

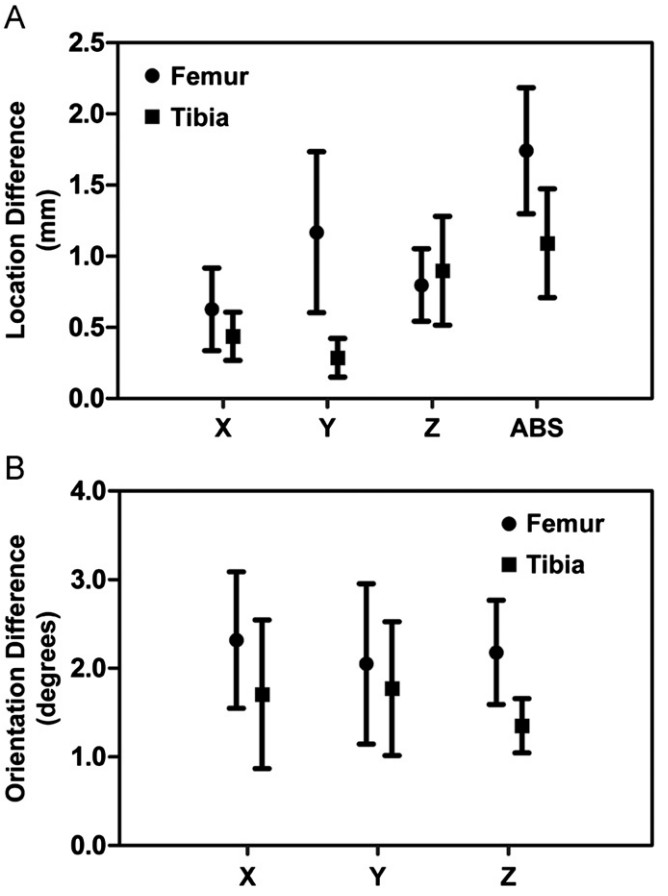

Fig. 4. (A) Average location variability of the ACS origins in mm. (B) Average orientation variability of the ACS axes in degrees. Circles correspond to the femur ACSs and squares correspond to the tibia ACSs. Error bars are 95% confidence intervals. Variability between the ACSs is thought to be influenced primarily by differences in bone morphology between specimens.

condyles was used to build the knee's FE axis (Fig. 2B). Additionally, the axis through the femoral diaphysis (anatomical axis) was used in conjunction with the "cylindrical axis" to create the third axis of the femoral ACS. As a result of the cross-product the third axis of the femoral ACS is tilted medially, pointing from the center of the condyles toward the femoral head (Fig. 1A.1). However, these observations require further quantitative investigation.

While the ACSs were designed with traditional definitions in mind, the absence of hip and ankle data combined with the lack of any gold standard complicate the evaluation of the proposed method. McPherson et al. described a method for creating a JCS for the distal femur and proximal tibia; however, the method is based on an extended knee position and assumes no variation of relative position between the femur and tibia between individuals. This assumption may not hold when investigating abnormal knee mechanics (McPherson et al., 2005). In these cases, a subject-specific method for creating position-independent femoral and tibial ACSs is necessary.

The algorithm's repeatability with regard to subject-specific ACSs was evaluated by comparing inter-specimen ACSs. The majority of variability was likely a consequence of between-subject morphology differences. These differences contributed to increased variability because exact bone morphology was used to build the ACSs. Furthermore, surface discrepancies between specimens visibly affected the surface registration technique, creating imperfections in the alignment that contributed to increased variability. While only one template knee position was used, this evaluation emphasizes the proposed method's sensitivity to the anatomical and morphological differences between specimens, highlighting its capability of generating consistent subject-specific ACSs.

An essential component of the femoral ACS is the smallest inertial axis of the femoral diaphysis (Fig. 2A.2). This axis is consistently oriented through the diaphysis; however, its orientation is affected when the diaphyseal length approaches its width. We determined that a length larger than $\sim$55 mm consistently orients the inertial axes with deviations less than 1°. In circumstances where the diaphyseal length approaches its diameter, the smallest inertial axis may be oriented in many directions. In these circumstances, it is appropriate to use the center axis of a cylinder fit to the diaphysis. The average diaphysis length used in this study was 146 ± 21 mm.

Accurately capturing all three anatomical planes of the knee is the first step in the assessment of knee kinematics. Differences between the presented ACS definitions and previous methods will likely result in slightly different kinematic interpretations; however, an attempt to minimize these differences was made by translating traditional axis definitions. While differences are unavoidable, providing a clear definition is required to interpret joint motion (Most et al., 2004). Herein, we defined the first, second, and third axes for the femur and tibia ACSs in detail.

Conflict of interest

None.

Acknowledgments

The authors would like to acknowledge their funding sources: NIH COBRE P20 RR024484, RIH Orthopaedic Foundation, Inc., and The W.M. Keck Foundation.

References

Andriacchi, T.P., Mündermann, A., Smith, R.L., Alexander, E.J., Dyrby, C.O., Koo, S., 2004. A framework for the *in vivo* pathomechanics of osteoarthritis at the knee. Ann. Biomed. Eng. 32 (3), 447–457.

Andriacchi, T.P., Mündermann, A., 2006. The role of ambulatory mechanics in the initiation and progression of knee osteoarthritis. Curr. Opin. Rheumatol. 18 (5), 514–518.

Andriacchi, T.P., Koo, S., Scanlan, S.F., 2009. Gait mechanics influence healthy cartilage morphology and osteoarthritis of the knee. J. Bone Joint Surg. Am. 91 (Suppl. 1), 95–101.

Eckhoff, D.G., Bach, J.M., Spitzer, V.M., Reinig, K.D., Bagur, M.M., Baldini, T.H., Flannery, N.M.P., 2005. Three-dimensional mechanics, kinematics, and morphology of the knee viewed in virtual reality. J. Bone Joint Surg. Am. 87 (Suppl. 2), 71–80.

Fernandez, J.W., Akbarshahi, M., Kim, H.J., Pandy, M.G., 2008. Integrating modelling, motion capture and x-ray fluoroscopy to investigate patellofemoral function during dynamic activity. Comput. Methods Biomech. Biomed. Eng. 11 (1), 41–53.

Gonzalez-Ochoa, C., McCammon, S., Peters, J., 1998. Computing moments of objects enclosed by piecewise polynomial surfaces, ACM TOG.

Jordan, S.S., DeFrate, L.E., Nha, K.W., Papannagari, R., Gill, T.J., Li, G., 2007. The *in vivo* kinematics of the anteromedial and posterolateral bundles of the anterior cruciate ligament during weightbearing knee flexion. Am. J. Sports Med. 35 (4), 547–554.

McPherson, A., Kärrholm, J., Pinskerova, V., Sosna, A., Martelli, S., 2005. Imaging knee position using MRI, RSA/CT and 3D digitisation. J. Biomech. 38 (2), 263–268.

Morrison, J.B., 1970. The mechanics of the knee joint in relation to normal walking. J. Biomech. 3 (1), 51–61.

Most, E., Axe, M.J., Rubash, H., Li, G., 2004. Sensitivity of the knee joint kinematics calculation to selection of flexion axes. J. Biomech. 37 (11), 1743–1748.

Pennock, G.R., Clark, K.J., 1990. An anatomy-based coordinate system for the description of the kinematic displacements in the human knee. J. Biomech. 23 (12), 1209–1218.